Evaluation of TAMDAR Data Impact on Forecast Error with WRFDA-FSO System

Xiaoyan Zhang, Xiang-Yu Huang, Xin Zhang, Feng Gao, Tom Auligne

NCAR Earth System Laboratory, Boulder CO

Neil A. Jacobs and Peter Childs
AirDat LLC

1 Introduction:

As an important part in the global observing system, the Aircraft data have been shown the progressive performance in the regional and global data assimilation systems (Benjamin et al. 1999; Benjamin 1995; Drtie et al. 2008, DiMego et al. 1992). With the newer feature than other aircraft data, TAMDAR (Tropospheric Aircraft Meteorological Data Reports) measures not only wind and temperature, but also the humidity, turbulence, and icing which were not available in other most of the aircraft data. That is why TAMDAR is rapidly becoming a major source of critical data utilized by various assimilation systems for the improvement of mesoscale NWP and the overall safety of aviation in the future (Fischer 2006). It is worth to strengthen that TAMDAR data routinely complete the absence of in-situ humidity observations, which only collected by the scattered radiosonde soundings (RAOB); by equipping regional aircraft, TAMDAR data cover the entire North America, including Alaska and Mexico, and generate data from locations and times not available from any other system (Gao, 2011); the aircraft with TAMDAR cruise at the moisture resides area and the convective activity region that is generally below 25000 feet (Daniels et al. 2006).

Moninger et al. (2010) had demonstrated that the assimilation of TAMDAR observations improves 3h RUC forecasts in the region and altitude range where the TAMDAR flies, especially the 3-h relative humidity forecast errors are reduced by up to 3% RH. Gao et. al (2011) also presented that the assimilation of TAMDAR observations in WRFDA (the Weather Research & Forecasting model Data Assimilation) system improve the 20-km 24-h WRF forecast. In this paper, we are going to evaluate the contribution of TAMDAR to reduce the 24-h forecast error comparing with other conventional observations by the WRFDA Forecast Sensitivity to Observation (FSO) system. The WRFDA-FSO is an extensive system of WRFDA for evaluating the quality

of observation impact on forecast. It is adjoint-based observation sensitivity techniques, which have been discussed and used by Baker and Daley, 2000; Cardinali and Buizza, 2004; Langland and Baker, 2004; Morneau et al., 2006; Xu et al., 2006; Errico, 2007; Zhu and Gelaro, 2008; Cardinali, 2009; to measure the observation impact evaluated with respect to a scalar function representing the short-range forecast error.

The aim of this paper is to illustrate the type of investigation and diagnostics for TMADAR and other conventional data that can be carried out with the adjoint-based observation sensitivity in WRFDA-FSO. In section 2, the theoretical background of the forecast sensitivity and the WRFDA-FSO system will be briefly introduced. Results are illustrated in section 3 and conclusions are given in section 4.

2 Formulation of WRFDA-FSO system

The study by Langland and Baker (2004) describes the use of an adjoint-based measure for estimating the impact of observations on numerical weather forecasts. The measure requires adjoints of both the forecast model and data assimilation system to estimate efficiently the reduction in forecast error due to arbitrary subsets of observations used by the data assimilation system. The WRFDA-FSO system has been developed since 2008 (Auligne, 2010) based on the WRFDA system and the WRF tangent linear and adjoint model (WRFPLUS). The WRF adjoint model can be used to calculate the adjoint sensitivity of short range WRF forecast errors to the initial conditions. In order to conduct adjoint sensitivity studies, a forecast error is defined as:

$$e = (\mathbf{x}^f - \mathbf{x}^t)^T \mathbf{C} (\mathbf{x}^f - \mathbf{x}^t) \quad (1)$$

where $\mathbf{C}$ is a symmetric, usually diagonal, matrix of weights and the superscript T denotes the transport operation. $\mathbf{x}^f$ is the forecast from initial conditions with the nonlinear model. According to Gelaro et al. (2007), the first-, second- and third-order approximations of the predefined forecast error Eq. (1), respectively, are

$$\delta e_1 = 2(\mathbf{x}_a - \mathbf{x}_b)^T \mathbf{M}_b^T C(\mathbf{x}_a^f - \mathbf{x}^t) \quad (2)$$

$$\delta e_2 = (\mathbf{x}_a - \mathbf{x}_b)^T [\mathbf{M}_b^T C(\mathbf{x}_a^f - \mathbf{x}^t) + \mathbf{M}_a^T C(\mathbf{x}_b^f - \mathbf{x}^t)] \quad (3)$$

$$\delta e_3 = (\mathbf{x}_a - \mathbf{x}_b)^T [\mathbf{M}_b^T C(\mathbf{x}_b^f - \mathbf{x}^t) + \mathbf{M}_a^T C(\mathbf{x}_a^f - \mathbf{x}^t)] \quad (4)$$

In Eqs (2)-(4), $\mathbf{x}_b^f$ and $\mathbf{x}_a^f$ are forecasts initialized from the background $\mathbf{x}_b$ and the analysis $\mathbf{x}_a$ at initial time; $\mathbf{M}_b^T$ and $\mathbf{M}_a^T$ are the matrices of the WRF adjoint model based on the forecast trajectories from the nonlinear evolution of $\mathbf{x}_b$ and $\mathbf{x}_a$ respectively. Eqs. (2)-(4) provide first-, second- and third-order approximations of the change in the error from $\mathbf{x}_a^f$ to $\mathbf{x}_b^f$, typically a reduction in forecast error due to improved initial conditions. In the third-order approximation (4), two augmented forms, denoted δe_4 and δe_5, are given in Gelaro et al. (2007) as

$$\delta e_4 = (\mathbf{x}_a - \mathbf{x}_b)^T [\mathbf{M}_a^T C(\mathbf{x}_b^f - \mathbf{x}^t) + \mathbf{M}_a^T C(\mathbf{x}_a^f - \mathbf{x}^t)] \quad (5)$$

and

$$\delta e_5 = (\mathbf{x}_a - \mathbf{x}_b)^T [\mathbf{M}_b^T C(\mathbf{x}_b^f - \mathbf{x}^t) + \mathbf{M}_b^T C(\mathbf{x}_a^f - \mathbf{x}^t)] \quad (6)$$

In the calculation of δe_4, the operator $\mathbf{M}_b^T$ in the first term of (4) has been replaced with the operator $\mathbf{M}_a^T$, while in δe_5, the operator $\mathbf{M}_a^T$ in the second term of (4) has been replaced with the operator $\mathbf{M}_b^T$. These substitutions are effectively equivalent to assuming the forecast model is linear in that the distinction between $\mathbf{M}_a^T$ and $\mathbf{M}_b^T$ has been ignored.

Once the forecast sensitivity is computed, the forecast sensitivity equation with respect to the observation in the context of variational data assimilation is derived as Baker and Daley (2000). The sensitivity of *e* with respect to the observations can be written using a simple derivation chain as:

$$\frac{\partial e}{\partial \mathbf{y}} = \frac{\partial e}{\partial \mathbf{x}_a} \frac{\partial \mathbf{x}_a}{\partial \mathbf{y}} \quad (7)$$

where $\partial e / \partial \mathbf{x}_a$ is the sensitivity of the forecast error described in equation (2)-(6) to the initial condition. As to $\partial \mathbf{x}_a / \partial \mathbf{y}$, it can be solved by the adjoint of WRFDA 3D-Var system corresponding to the innovation $\delta \boldsymbol{y}$.

In this paper, we used the latest version of WRFDA-FSO system (Figure 1.), including WRF Model V3.3.1, WRF-DA V3.3.1 and the new upgraded WRFPLUS based on the WRF model V3 (Zhang, 2010). The parallel performance of WRFPLUS was greatly optimized **in** the summer of 2011. Although WRFPLUS includes the simplified vertical diffusion, Kessler microphysics and simplified cumulus scheme, moist physical processes are not included in this paper. So the forecast error is

calculated with only the dry energy norm. Considering the accuracy, in this paper, we adopt the third-order sensitivity but in the manner of equation (5).

3 Results of the forecast error reduction

The impacts of TAMDAR and other conventional observations on 24-hour forecasts as measured by Eqs. 5 & 7 are examined for the month of January and June 2010 using WRFDA-FSO system. Analyses ($\mathbf{x}_a$) are produced by WRFDA three-dimensional variational (3D-Var) at 60km horizontal resolution, and 35 vertical levels defined in sigma coordinates with a top of 50 hPa using 6-hour interval cold-start that includes all conventional observations except for satellite radiances. The conventional observation includes raobs, synop, metar, pilot, profiler, airep, ship, buoy, gpsref, gpspw, satellite retrieval wind and TAMDAR. The background fields of WRFDA 3D-Var is the WRF 6-hour forecast from NCEP FNL. It is the cold-start data assimilation with the 6-hour interval every day. The 24-hour WRF forecasts trajectory were performed on the same model configuration as WRFDA 3D-Var on a single 400 x 250 grid that covered the US and surrounding oceanic regions (Figure 2) from the 00, 06, 12, 18 UTC analysis ($\mathbf{x}_a$) and corresponding background stat ($\mathbf{x}_b$) for each day of the study period. In this study, the Kain-Fritsch cumulus parameterization was employed (Kain 2004), along with the Goddard cloud microphysics scheme, and the Yonsei University (YSU) planetary boundary layer parameterization (Hong et al. 2006). Adjoint forecasts along these trajectories are produced by WRF adjoint model (WRFPLUS) at this same horizontal and vertical resolution but without physics scheme. The starting conditions for the adjoint forecasts are $\partial e/\partial \mathbf{x}^f$, computed as indicated on the right sides of Eq. (5). The output fields from the adjoint model forecasts, in turn, are used as starting conditions for the WRFDA 3D-Var adjoint. This adjoint is an exact line-by-line adjoint run at the same resolution and with the same observation set used to produce $\mathbf{x}_a$. A post-processing procedure was integrated in WRFDA, which is applied to compute the inner product between the output of the WRFDA 3D-Var adjoint and the innovations $\delta \boldsymbol{y}$ to produce the various-order observations-space approximation of δe. All the experiments were performed using the third-order sensitivity gradient defined in Eq. (5).

3.1 June

The impact of the conventional dataset on the 24-hour forecast error has been investigated from 1 to 25 June 2010 at 00, 06, 12, 18 UTC. The average performance over the near month is summarized in Figure 3. Negative values correspond to a decrease of forecast error due to a specific observation type. The largest error decrease is due to TAMDAR and Sound followed by GeoAMV, METAR, GPSREF and SYNOP. It is surprised that the error reduction of TAMDAR is a little greater than Sound. But it is really proved by more detailed diagnostic of the forecast error contribution from different times and different vertical levels. Figure 4 is the performance in Figure 3 divided by observation numbers, which presents the contribution of error reduction from TAMDAR is less than Sound comparing with Figure 3. This averaged forecast error reduction over each observed point means the single contribution from TAMDAR is less than Sound. Combining Figure 3 and 4, it can be concluded that the largest contribution to reduce the 24-hour forecast error from TAMDAR is due to its denser coverage in both horizontal and vertical than Sound. For further understanding, a period of time series of observation number of TAMDAR and Sound that assimilated in WRFDA 3D-Var is shown in Figure 5. The truth is the number of TAMDAR is quite more than Sound at every assimilation time, especially at 1800 UTC when the radio sound report is absent. Correspondingly, Figure 6 is the time series of error reduction in the same period as Figure 5, which proves the TAMDAR has the absolutely advantage at 1800 UTC to reduce the 24-hour forecast error. The forecast error reduction of Sound at 0000 and 1200 UTC is slightly greater than TAMDAR or equivalent at some days. At 1800 UTC, however, TAMDAR contributes similar error reduction as at 0000 and 1200 UTC, but very tiny contribution from a few drop sounds. Therefore, the priority of TAMDAR in Figure 3. mostly come from the contribution of 1800 UTC observation.

More detailed diagnostic of the forecast error contribution at vertical level from TAMADR and Sound is shown in Figure 7 (0000 UTC) and Figure 8 (1800 UTC). The observed variables (U, V, T, Q) are grouped by pressure levels. The degradation of T and Q from TAMDAR at 850- and 700-hPa is much more than Sound at both 0000 and 1800 UTC. Again, each observed variable of TAMDAR has absolutely advantage to reduce the

forecast error at lower level at 1800 UTC comparing with Sound. Apparently, assimilation of TAMDAR RH observations improves the 24-h WRF 60-km forecast in cases in the middle troposphere. That makes up the big gap where and when lack the moisture observations. That might be the biggest contribution of TAMDAR observation to regional WRF forecast.

3.2 January

The winter period examined in this paper ranges from 1 to 30 January. On the 24-hout forecast error the observation performance (Figure 9) is very similar to the summer one shown in Figure 3. The forecast error reduction for TAMDAR, Sound and GeoAMV show the common seasonal variations with smaller negative value in the winter and bigger errors in summer, when the lower troposphere is more commonly well mixed with a deeper boundary layer. More detailed analysis of moisture forecast error is displayed in Figure 10, which grouped the water vapor mixing ratio (Q) forecast error reduction with pressure levels at 0000, 0600, 1200 and 1800 UTC respectively. Obviously, TAMDAR observation has the absolutely superiority comparing with Sound to on reducing the lower level 24-hour moisture forecast error at 0000, 0600 and 1800 UTC, except for the 1200 UTC. The reason is Sounding observation has more data than TAMDAR at 1200 UTC. Recalling the Q forecast error reduction in Figure 8, we find the winter Q forecast error is smaller than it in summer too. It is another reflection that the RH observation from TAMDAR benefits to the convective activity which happened more in summer than winter.

4 Conclusions

This paper illustrates the use of the forecast sensitivity with respect to observational data in a 6-hour 3D-Var assimilation system, as a diagnostic tool to monitor the observation performance in the short-range forecast. The WRFDA-FSO system is examined over the CONUS domain through 2-month (winter and summer) 60km run. The basic FSO diagnostic for conventional results show that the greatest error reduction comes from the wind and temperature observations. In term of observation type, the largest error reduction is headed by TAMDAR and Sound, followed by GeoAMV,

METAR, GPSREF and SYNOP. The contribution of TAMDAR observation to reduce the forecast error is analyzed in detail. All the wind, temperature, and relative humidity of TAMDAR have very impressive contribution in WRFDA-FSO system, especially the humidity. The features of TAMDAR observation that studied in previous research is proved through this study. That include:

•TAMDAR data has obvious contribution on 1800 UTC to reduce the 24-hour forecast error, which makes the TAMDAR observation leads the largest forecast error reduction when only conventional observation assimilated.

•TAMDAR relative humidity data is a very important supplementary of sounding data at lower level roughly below 500 hPa. It is very important to capture the better short-range forecast for convective system

•Dense data coverage is another benefit from TAMDAR that has much more data than Sound at 0000 , 0600, 1200, especially at 1800 UTC.

5 Reference

AULIGNE, T. et al., 2010: Forecast Sensitivity to Observations and Observation Impact. WRFDA Tutorial, Boulder CO, August 3-5 2010. Available online at: [http://www.mmm.ucar.edu/wrf/users/wrfda/Tutorials/2010_Aug/docs/WRFDA_sensitivity.pdf]

Baker, N. and R. Daley, 2000: Observation and background adjoint sensitivity in the adaptive observation-targeting problem. Quart. J. Roy. Meteor. Soc., **126**, 1431–1454.

Cardinali, C. and R. Buizza, 2004: Observation sensitivity to the analysis and the forecast: A case study during atrec targeting campaign. Proceedings of the first THORPEX international science symposium, Montreal, Canada, 000–000.

Cardinali, C., 2009: Monitoring the observation impact on the short-range forecast. Quart. J. Roy. Meteor. Soc., **135**, 239–250.

Daniels, T. S., W. R. Moninger, and R. D. Mamrosh, 2006: Tropospheric Airborne Meteorological Data Reporting (TAMDAR) Overview. 10th Symposium on Integrated Observing and Assimilation Systems for Atmosphere, Oceans, and Land Surface (IOAS-AOLS), AMS, Atlanta, GA.

ER R I C O, R. M. , 2007: Interpretations of an adjoint-derived observational impact measure. Tellus **59A**, 273–276.

Gao, F., X-Y. Zhang, N. Jacobs, X-Y. Huang, X. Zhang, and P. Child, 2011: Estimation of TAMDAR Observational Error and Assimilation Experiments. *Wea. Forecasting*, in review.

GE L ARO, R. , Y. ZHU, R. M. ER R I C O, 2007: Examination of various-order adjoint-based approximations of observation impact. – Meteorol. Z. **16**, 685–692.

Helms, D., and Coauthors, 2005: NOAA's deployment of the Water Vapor Sensor System (WVSS II). Preprints, 21st Conf. on Weather Analysis and Forecasting/17th Conf. on Numerical Weather Prediction, Washington, DC, Amer. Meteor. Soc., P1.45. Available online at: [http://www.nws.noaa.gov/ost/wvss/AMS_NWP-WVSSII_Poster_JUL05.pdf]

Langland RH, Baker NL. 2004. Estimation of observation impact using the NRL atmospheric variational data assimilation adjoint system. *Tellus* **56A**: 189–201.

Moninger, W. R., S. G. Benjamin, B. D. Jamison, T. W. Schlatter, T. L. Smith, and E. J.Szoke, 2010: Evaluation of Regional Aircraft Observations Using TAMDAR. *Wea. Forecasting*, **25**, 627–645.

Morneau J, Pellerin S, Laroche S, Tanguay M. 2006. 'Estimation of adjoint sensitivity gradients in observation space using the dual (PSAS) formulation of the Environment

Canada operational 4DVar.' Pp. 162–163 in Proc. Second THORPEX international Science symposium, 4–8 December 2006, Landshut, Germany. WMO/TD No. 1355, WWRP/THORPEX No. 7.

Xu L, Langland R, Baker N, Rosmond T. 2006. 'Development and testing of the adjoint of NAVDAS-AR.' Seventh international workshop on adjoint applications in dynamic meteorology, 8–13, October 2006, Obergurgl, Austria.

Zhang, X. , Recently upgrades and improvements of WRF 4D-Var system. http://ams.confex.com/ams/91Annual/webprogram/Paper182521.html

Zhu Y, Gelaro R. 2008. Observation sensitivity calculations using the adjoint of the Gridpoint Statistical Interpolation (GSI) analysis system. *Mon. Weather Rev.* **136**: 335–351.

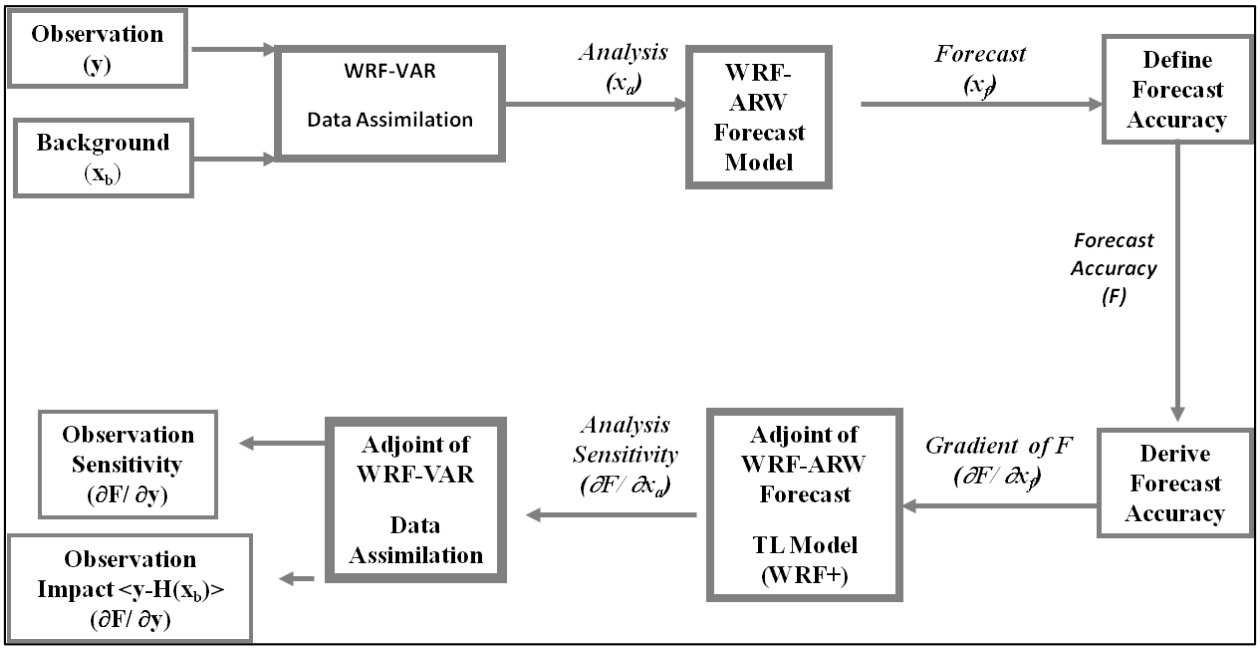

Figure 1. Schematic of the procedure to run Forecast Sensitivity to Observations

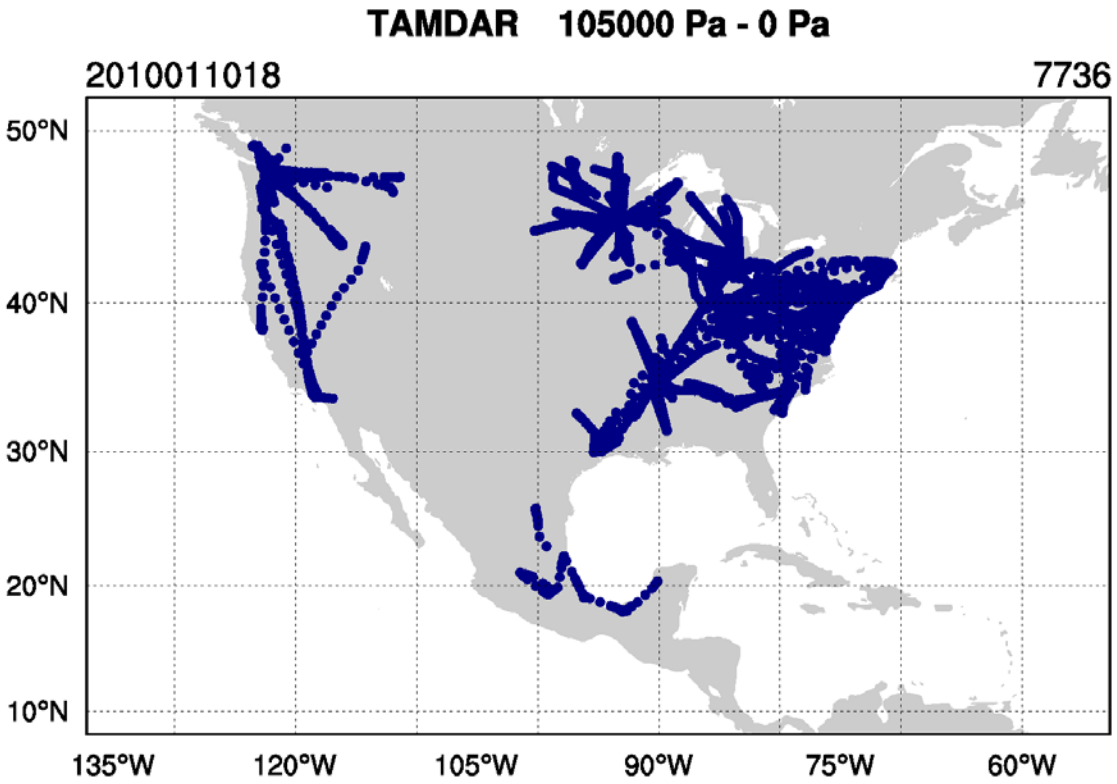

Figure 2. The model configuration (The blue dots is an example of the coverage of TAMDAR observation at 1800 UTC).

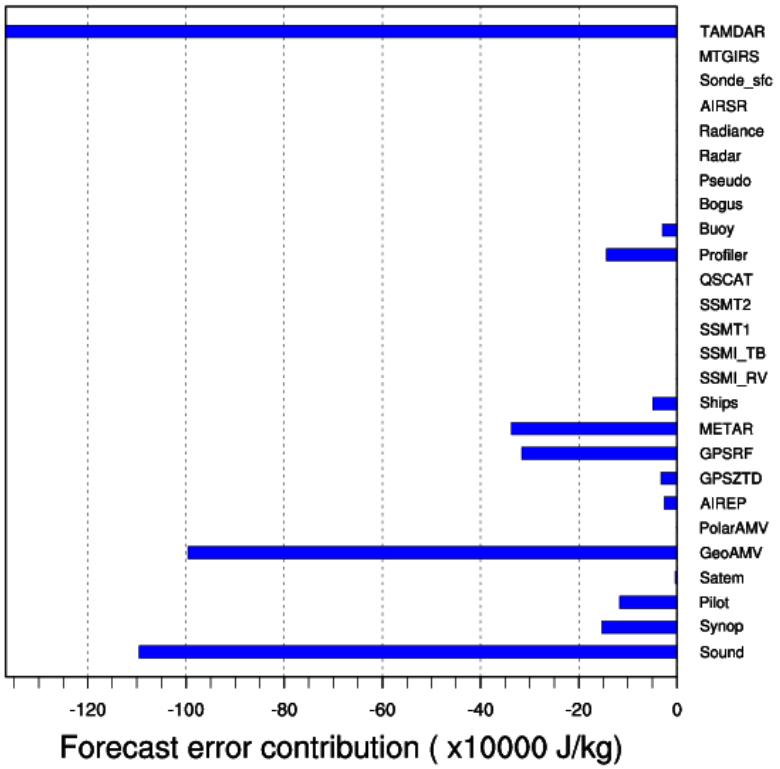

Figure 3. 24-hour forecast error contribution in J/kg of the types of observing system in **June** 2010. Negative values correspond to a decrease in the energy norm of forecast error.

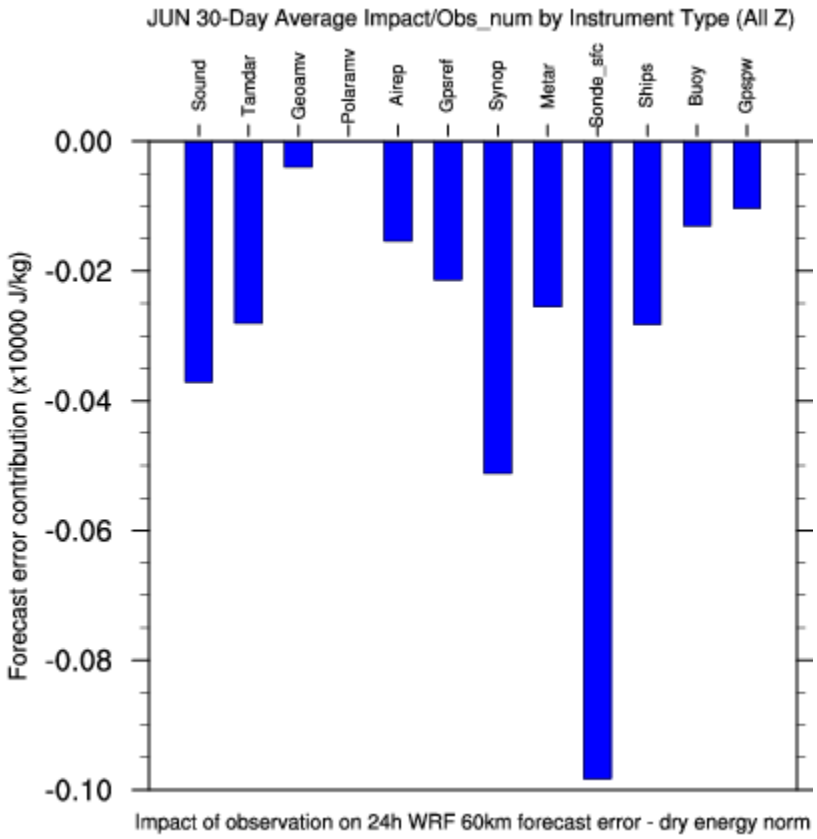

Figure 4. Similar to Figure 3. , but divided by the observation number

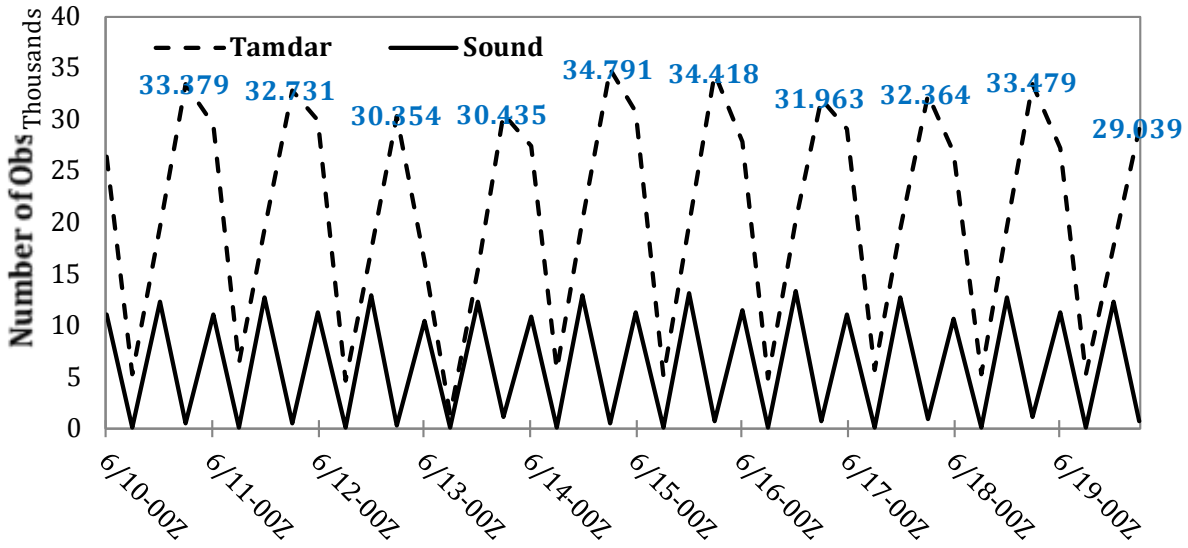

Figure 5. The time series for the number of Tamdar (dash line) and Sound (solid line) assimilated every 6-hour in WRFDA 3D-Var from 10 to 19 **June** 2010

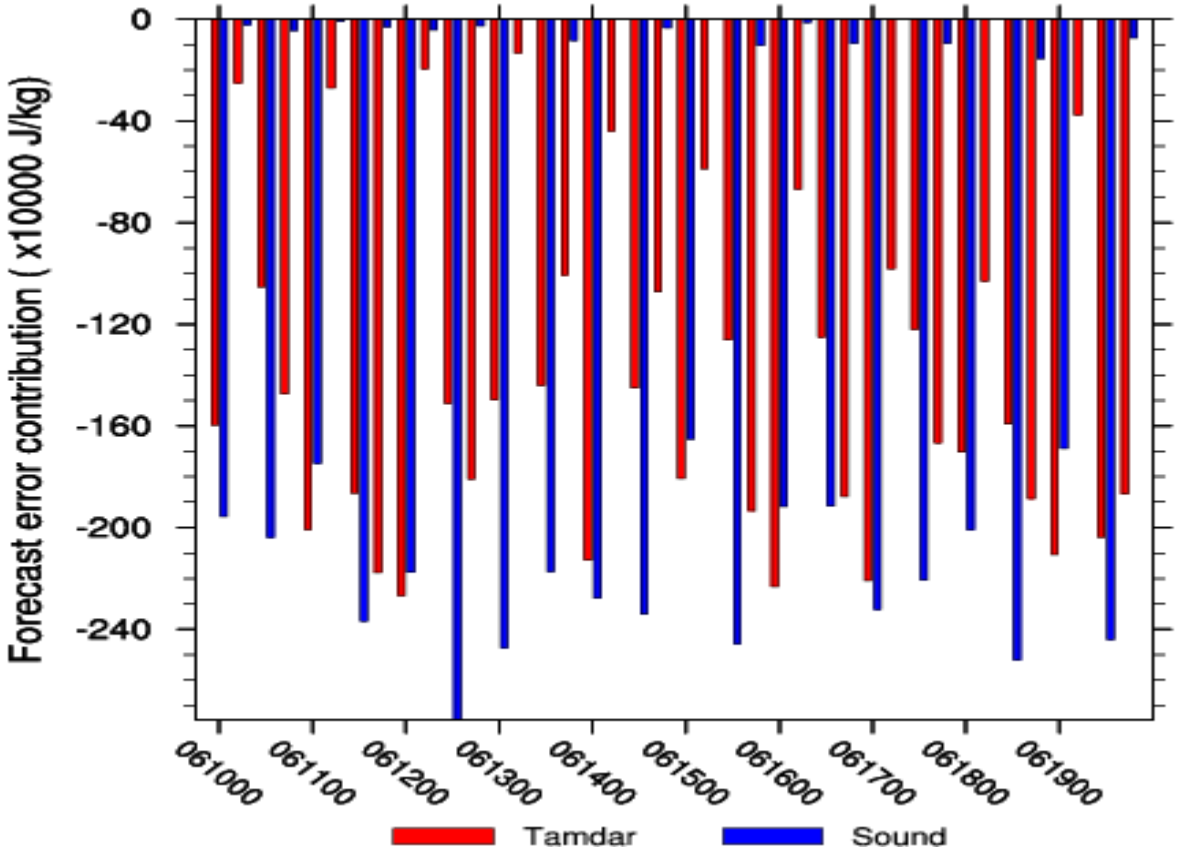

Figure 6. The time series for the forecast error reduction from 0000 UTC 10 to 1800 UTC 19 **June** 2010.

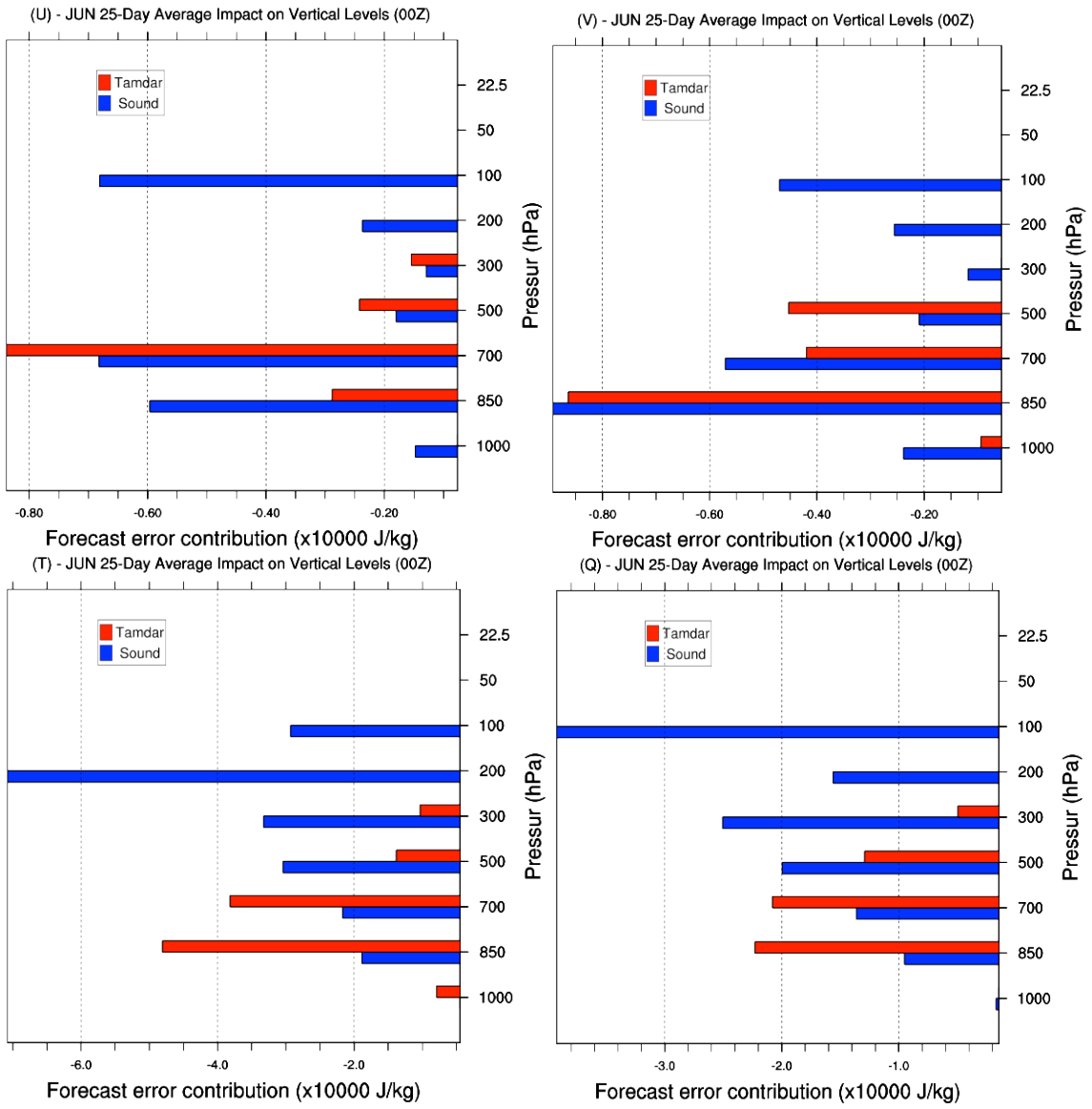

Figure 7. 24-hour forecast error contribution of the observed variables on pressure levels (hPa) and grouped by TAMDAR (red) and Sound (blue), averaged from 2 – 25 **June** at 0000 UTC.

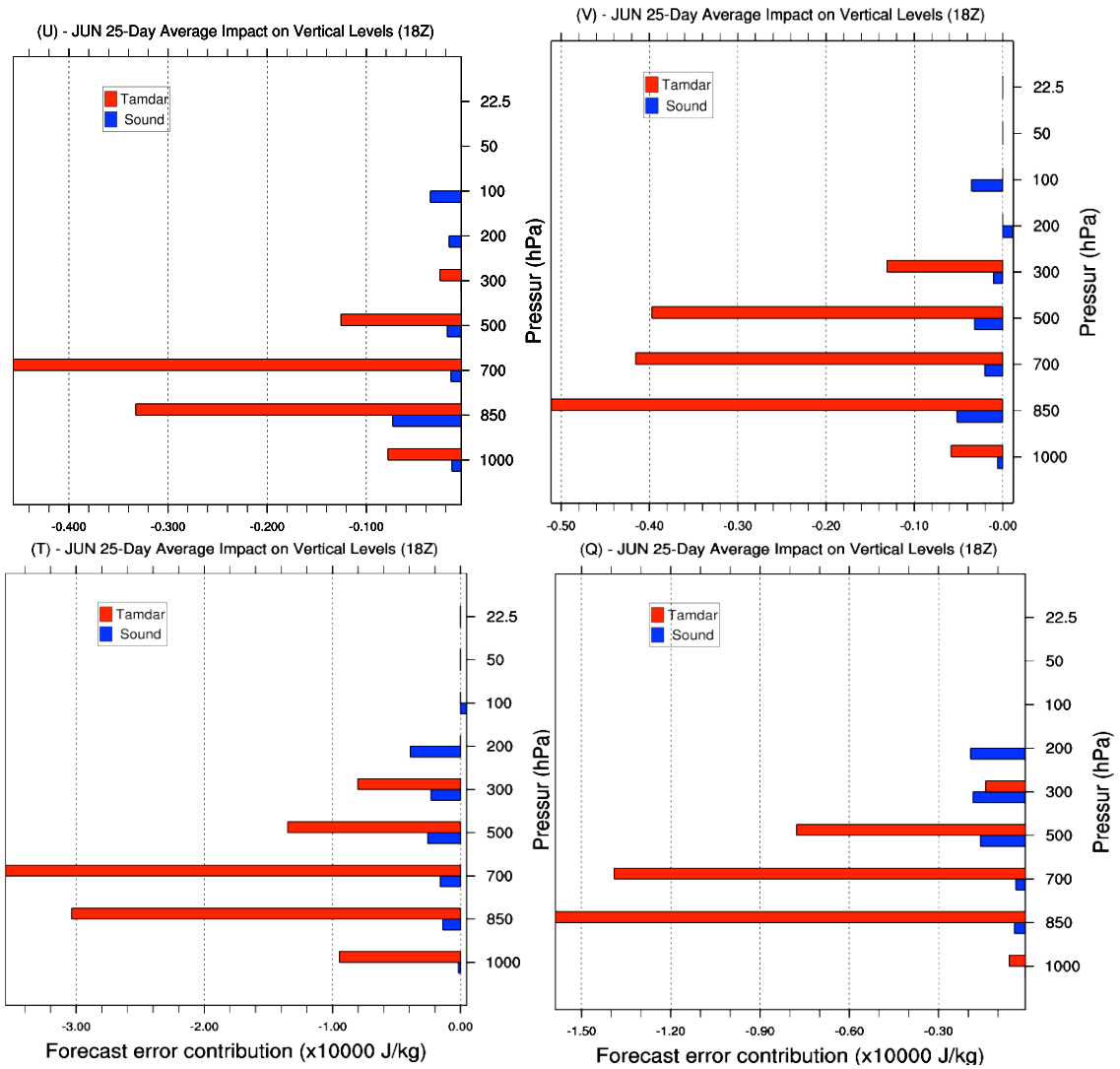

Figure 8. 24-hour forecast error contribution of the observed variables on pressure levels (hPa) and grouped by TAMDAR (red) and Sound (blue), averaged from 1 – 24 **June** at 1800 UTC.

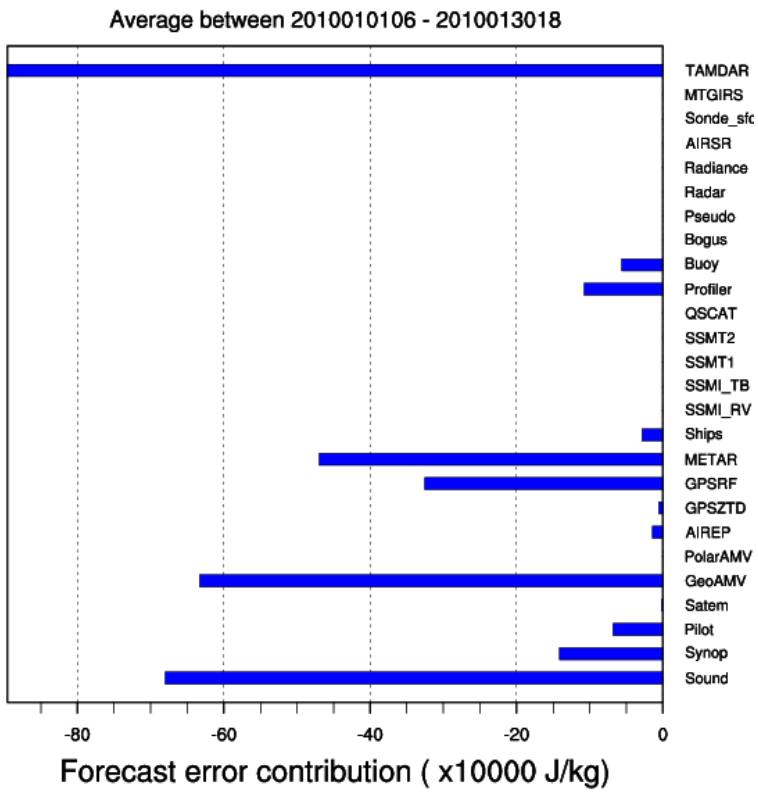

Figure 9. 24-hour forecast error contribution (J/kg) of the types of observing system in **January** 2010. Negative values correspond to a decrease in the energy norm of forecast error.

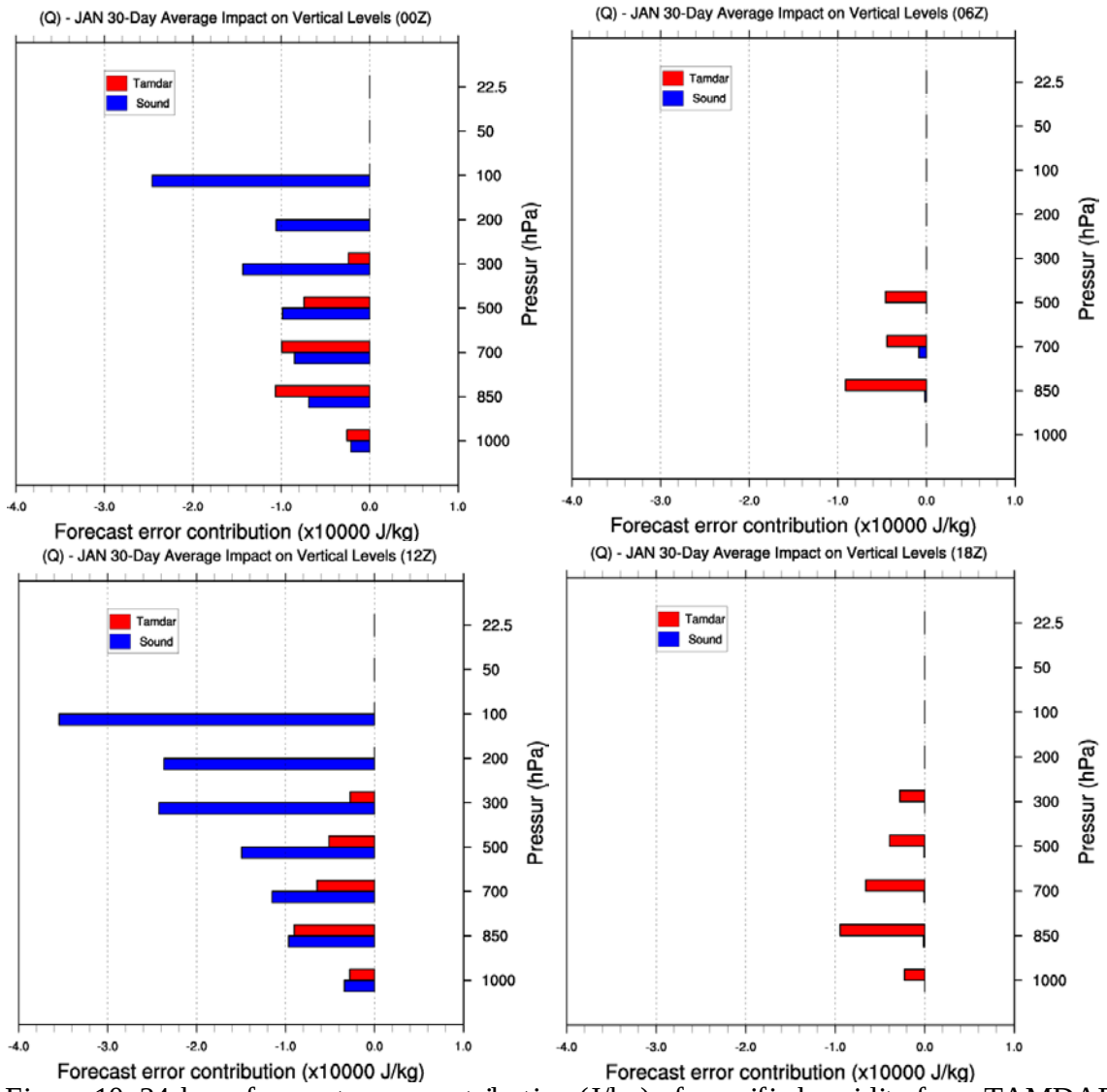

Figure 10. 24-hour forecast error contribution (J/kg) of specific humidity from TAMDAR (red) and Sound (blue) at different vertical levels in **January** 2010, from 1000 hPa above the surface up to 50 hPa.